Inorg. Chem. **2009**, *48*, 1507−1518

Solution Structure and Dynamics, Stability, and NIR Emission Properties of Lanthanide Complexes with a Carboxylated Bispyrazolylpyridyl Ligand

Marta Mato-Iglesias,[†] Teresa Rodríguez-Blas,[†] Carlos Platas-Iglesias,*[,†] Matthieu Starck,[‡] Pascal Kadjane,[‡] Raymond Ziessel,[‡] and Loïc Charbonnière*[,‡]

Departamento de Química Fundamental, Universidade da Coruña, Campus da Zapateira, Alejandro de la Sota 1, 15008 A Coruña, Spain, and Laboratoire de Chimie Organique et Spectroscopie Avancées CNRS UMR 7515, ECPM-ULP, 25 rue Becquerel, 67087 Strasbourg Cedex 02, France

Received September 22, 2008

The complexation behavior of the ligand 2,6-bis{3-[*N*,*N*-bis(carboxymethyl)aminomethyl]pyrazol-1-yl}-pyridine, **L**, toward lanthanide cations was investigated throughout the series. Potentiometric titration experiments on **L** (0.1 M KCl) revealed the presence of four protonation steps in the 2−12 pH domain, associated with the protonation of the two tertiary amine nitrogen atoms and with two of the four carboxylate functions. The stability constants for the formation of the [Ln**L**]$^-$ complexes (Ln = La, Nd, Eu, Ho, and Lu) were determined in water and evidenced a hill-shaped complexation trend along the series, with log *K* increasing from 14.56(9) (La) to 16.68(2) (Ho) and decreasing to 15.42(2) (Lu). Geometry optimizations showed the [Ln**L**]$^-$ complexes (Ln = La, Nd, Eu, Ho, Yb, and Lu) adopting a C_2 symmetry with the symmetry axis going through the metal atom and the nitrogen atom of the central pyridine ring, leading to the presence of Δ and Λ helical enantiomers. Analysis of the calculated Ln−O and Ln−N bond lengths showed a marked deviation from the expected values at the end of the series, which accounts for the observed decreased complexation affinity. ^{1}H and ^{13}C NMR experiments in D_2O (room temperature) showed the shortening of the bond distances in [Ln**L**]$^-$ complexes from La to Lu to be accompanied by a rigidification of the structure, leading to a decreased C_2 symmetry for the Lu complex compared to C_{2v} for La. This decreased symmetry was attributed to a slow Δ ↔ Λ interconversion that was followed by variable-temperature ^{13}C NMR experiments on the Lu complex. The activation parameters determined by line broadening analysis for this interconversion process point to an associatively assisted interconversion process. The ^{1}H NMR spectrum of the paramagnetic [Yb**L**]$^-$ complex was investigated in D_2O, and a lanthanide induced shift analysis showed good agreement between the observed paramagnetic chemical shifts and those calculated from the DFT optimized structures using a dipolar model, especially when solvent effects are taken into account. The UV−vis absorption and near-infrared luminescence spectra of the Pr, Nd, Er, and Yb complexes were measured in water and showed the complexation pocket provided by the ligand to be well-suited for the protection of the cations, all of them displaying typical Ln-centered emission spectra, the Yb complex having a relatively long lifetime of 3.0 μs in water.

Introduction

The wide scope of applications of lanthanide complexes, for example, as contrast agents for magnetic resonance imaging[1] or as luminescent probes,[2] requires a fundamental understanding of the basic structural properties of such chelates. When a rational approach is applied to the design of chelates with predefined properties, a detailed knowledge

* To whom correspondence should be addressed. Tel.: (33) 3 90 24 26 90. Fax: (33) 3 90 24 27 42. E-mail: l.charbonn@chimie.u-strasbg.fr.
† Universidade da Coruña.
‡ Laboratoire de Chimie Organique et Spectroscopie Avancée.

(1) (a) Merbach, A. E.; Toth, E. In *The Chemistry of Contrast Agents in Medical Magneic Resonance Imaging*; Wiley: London, 2001. (b) Lauffer, R. B. *Chem. Rev.* **1987**, *87*, 901.
(2) (a) Bünzli, J.-C. G.; Piguet, C. *Chem. Soc. Rev.* **2005**, *34*, 1048. (b) Pandya, S.; Yu, J.; Parker, D. *Dalton Trans.* **2006**, 2757.

10.1021/ic801816p CCC: $40.75
Published on Web 01/16/2009

of the structure/activity relationships for different classes of lanthanide complexes is required, along with a deep understanding of the impact of changes in the chemical structure on these properties. Taking advantage of this knowledge, it becomes possible to design complexing entities providing a good shielding of the cation for luminescent labels,[3] or easy access of the solvent molecules or anions for Gd-based relaxation agents[4] or luminescent anion probes.[5] Much effort has been devoted to such studies with polyaminocarboxylate-based ligands such as ethylenediaminetetracarboxylic acid (EDTA), diethylenetriamine pentacarboxylic acid (DTPA), or 1,4,7,10-tetraazacyclododecane-N,N′,N″,N‴-tetraacetic acid, in order to understand the principles governing the water exchange rates of their Gd complexes.[6] However, in the case of luminescent lanthanide complexes, the larger synthetic efforts necessary for the introduction of the heteroaromatic sensitization moieties, the antenna,[7] often limit the available quantities of compounds. Investigations are then rather focused on less compound-consuming spectroscopic studies than on greedy experiments such as potentiometric or pH-metric titrations. Apart from simple chelating units,[8] or seldom for sophisticated compounds,[9] the basic physico-chemical properties of photosensitizing ligands are often underexamined.

Luminescent probes for bioanalytical applications require assemblies that are stable under physiological conditions, which contain suitable chromophoric groups and which can be coupled to biological material. Nevertheless, the introduction of rigid heteroaromatic moieties on the ligand backbone is responsible for severe constraints during the complexation process, from which the overall stability of the complex can drastically suffer. Within the course of our investigations on luminescent lanthanide complexes, we focused our attention on ligand **L** (Scheme 1), which was previously studied by Rodriguez-Ubis and co-workers and appeared to be an excellent photosensitizer for Eu and Tb.[10] Moreover, they also demonstrated that the replacement of the pyridine rings by other heterocyclic systems or their functionalization with appropriate groups affects the luminescent properties of the corresponding chelates but also provides a way to attach them to biomolecules.[11] Thus, this ligand can be considered a good candidate to be functionalized with groups able to couple with biological molecules for application in bioaffinity assays. However, while essential for biological applications, the stability, structure, and dynamics of the lanthanide complexes of **L** in aqueous solution remain unexplored.

Scheme 1

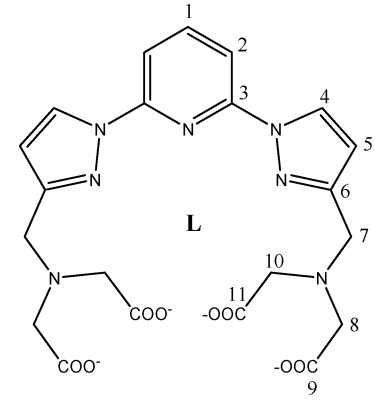

Herein, we report a detailed investigation of the complexes of **L** throughout the lanthanide series by using a combination of experimental and theoretical techniques. Thermodynamic stability constants of the complexes of this ligand have been determined by pH potentiometry. Aiming to rationalize the stability trend observed across the lanthanide series, the structure and dynamics of the complexes were studied by using ^{1}H and ^{13}C NMR techniques in a D_2O solution. In addition, the complexes were characterized by density functional theory (DFT) calculations carried out at the B3LYP level. The structures established by these calculations were compared with the structural information obtained in solution from paramagnetic NMR measurements (Yb-induced ^{1}H NMR shifts). Finally, we also demonstrate that **L** is an appropriate photosensitizer of near-infrared-emitting lanthanide cations such Pr, Nd, Er, and Yb.

Results and Discussion

Ligand Protonation Constants and Stability Constants of the Metal Complexes. The protonation constants of **L** as well as the stability constants with various Ln^{III} cations were determined by potentiometric titration. The constants and standard deviations are given in Table 1. The ligand protonation constants are defined as in eq 1, and the stability constants and the protonation constants of the complexes are expressed in eqs 2 and 3, respectively:

$$K_i = \frac{[H_iL]}{[H_{i-1}L][H^+]} \quad (1)$$

$$K_{ML} = \frac{[ML]}{[M][L]} \quad (2)$$

(3) Brunet, E.; Rodriguez-Ubis, J. C. *Curr. Chem. Biol.* **2007**, *1*, 11.
(4) (a) Aime, S.; Gianolio, E.; Barge, A.; Kostakis, D.; Plakatouras, I. C.; Hadjiliadis, N. *Eur. J. Inorg. Chem.* **2003**, 2045. (b) Caravan, P.; Amedio, J. C., Jr.; Dunham, S. U.; Greenfield, M. T.; Cloutier, N. J.; McDermid, S. A.; Spiller, M.; Zech, S. G.; Looby, R. J.; Raitsimring, A. M.; McMurry, T. J.; Lauffer, R. B. *Chem.—Eur. J.* **2005**, *11*, 5866.
(5) (a) Mameri, S.; Charbonnière, L.; Ziessel, R. *Inorg. Chem.* **2004**, *43*, 1819. (b) Charbonnière, L. J.; Ziessel, R.; Montalti, M.; Prodi, L.; Zaccheroni, N.; Boehme, C.; Wipff, G. *J. Am. Chem. Soc.* **2002**, *124*, 7779. (c) Bretonniere, Y.; Cann, M. J.; Parker, D.; Slater, R. *Org. Biomol. Chem.* **2004**, 1624. (d) Parker, D.; Yu, J. *Chem. Commun.* **2005**, 3141.
(6) Caravan, P.; Ellison, J. J.; Mc Murry, T. J.; Lauffer, R. B. *Chem. Rev.* **1999**, *99*, 2293.
(7) Weissmann, S. I. *J. Chem. Phys.* **1942**, *10*, 214.
(8) Comby, S.; Imbert, D.; Chauvin, A. S.; Bünzli, J.-C. G.; Charbonnière, L. J.; Ziessel, R. F. *Inorg. Chem.* **2004**, *43*, 7369.
(9) Senegas, J.-M.; Bernardinelli, G.; Imbert, D.; Bünzli, J.-C. G.; Morgantini, P.-Y.; Weber, J.; Piguet, C. *Inorg. Chem.* **2003**, *42*, 4680.
(10) (a) Remuinan, M. J.; Roman, H.; Alonso, M. T.; Rodriguez-Ubis, J. C. *J. Chem. Soc., Perkin Trans. 2* **1993**, 1099. (b) Brunet, E.; Juanes, O.; Sedano, R.; Rodriguez-Ubis, J.-C. *Photochem. Photobiol.* **2002**, *1*, 613.
(11) (a) Rodriguez-Ubis, J.-C.; Sedano, R.; Barroso, G.; Juanes, O.; Brunet, E. *Helv. Chim. Acta* **1997**, *80*, 86. (b) Brunet, E.; Juanes, O.; Sedano, R.; Rodriguez-Ubis, J.-C. *Tetrahedron Lett.* **2007**, *48*, 1091.

$$K_{MHL} = \frac{[MHL]}{[ML][H^+]} \quad (3)$$

The potentiometric curve of **L** (Figure S1, Supporting Information) is indicative of two fairly strong and two weak acidic sites. The data indicate that two protons are titrated below pH ~ 3.7, one between pH 3.7 and 8.5, and a fourth proton between 8.5 and 10.5. In comparison to EDTA,[12] **L** has a lower protonation constant for the first protonation step (Table 1), while the second protonation constant is ca. 1.8 log *K* units lower in EDTA than in **L**, these protonation processes likely occurring on the amine nitrogen atoms. The higher protonation constant for the second protonation step of **L**, in comparison to that of EDTA, is attributed to a lower electrostatic repulsion between the two protonated amine nitrogen atoms in **L** as a consequence of their larger separation. This result is in line with the higher log K_2 value observed for DTPA when compared to EDTA; the second log K_i in DTPA corresponds to the protonation of one of the terminal nitrogen atoms, with displacement of the first proton from the central to the other terminal nitrogen atom.[13] A comparison of the protonation constants of **L** with those of EDTA and DTPA suggests that the third and fourth protonation constants of **L** correspond to the protonation of carboxylate groups.

Potentiometric titrations of **L** have been carried out in the presence of equimolar amounts of Ln^{III} ions in order to determine the stability constants of the metal complexes. The 1:1 titration curves with metal ions (Figure S1, Supporting Information) display an inflection at $a = 4$ (a = moles of OH^-/moles of ligand), as expected for the formation of $[Ln\mathbf{L}]^-$ species. Monoprotonated forms of the complexes have been detected over the pH range studied for all of the Ln^{III} ions investigated. The species distribution diagram for the Eu^{III} complex (Figure 1) shows the presence of a monoprotonated complex in solution at pH < 6, while the dissociation of the complex occurs below pH ~ 4.

The log K_{ML} values obtained for **L** complexes increase along the Ln^{III} series from La^{III} to Ho^{III} ($\Delta\log K_{ML} = \log K_{HoL} - \log K_{LaL} = 2.08$) and finally decrease from Ho^{III} to Lu^{III} ($\Delta\log K_{ML} = \log K_{HoL} - \log K_{LuL} = 1.26$), while the

Table 1. Protonation Constants of **L** and EDTA and Stability Constants and pM[a] Values of Ln^{III} Complexes (Ln = La, Nd, Eu, Ho and Lu, 25 °C; I = 0.1 M (KCl))

	L	EDTA[b]		L	EDTA
log K_1	9.42(6)	10.17	pLa	12.8	13.6
log K_2	7.96(5)	6.11	pNd	14.3	14.7
log K_3	2.70(6)	2.68	pEu	14.4	15.5
log K_4	2.02(5)		pHo	14.9	16.8
			pLu	13.7	18.0
log K_{LaL}	14.56 (9)	15.46			
log K_{LaHL}	3.93(2)				
log K_{NdL}	16.03(1)	16.56			
log K_{NdHL}	3.22(1)				
log K_{EuL}	16.18(2)	17.32			
log K_{EuHL}	3.68(2)				
log K_{HoL}	16.68(2)	18.60			
log K_{HoHL}	3.44(2)				
log K_{LuL}	15.42(2)	19.80			
log K_{LuHL}	3.84(2)				

[a] pM values are usually defined as $pM = -\log[M]_{free}$ at pH = 7.4 for $[M^{III}] = 1\ \mu M$, $[\mathbf{L}] = 10\ \mu M$. [b] According to ref 12.

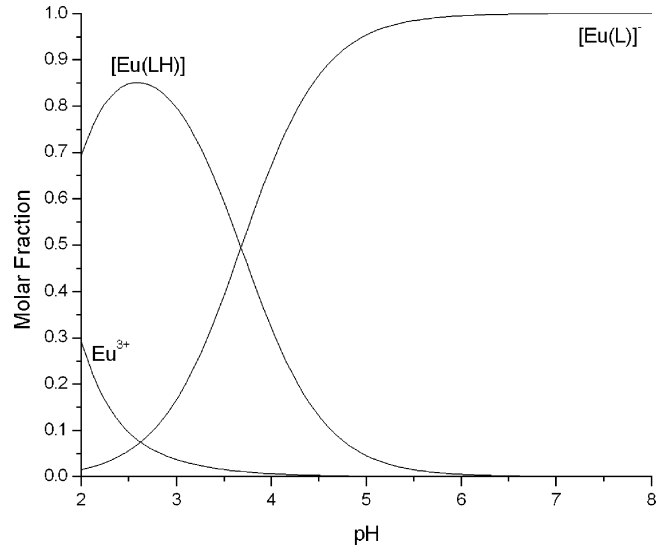

Figure 1. Species distribution of the Eu**L** system, 1:1 Eu^{III}/**L**; $[Eu^{III}] = 3$ mM, $\mu = 0.1$ M (KCl), 25 °C.

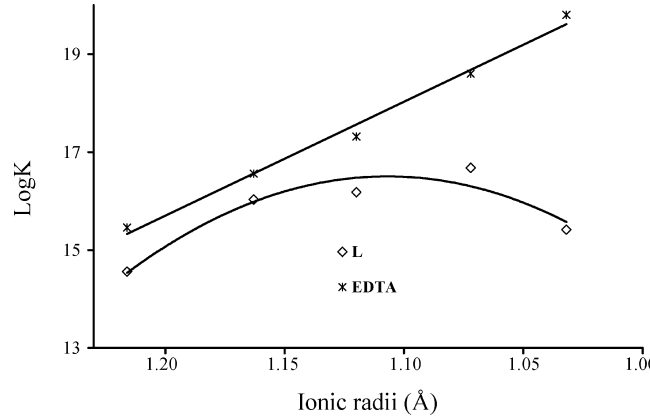

Figure 2. Evolution of the stability constants (log K_{ML} values) for **L** and EDTA as a function of the ionic radii of the lanthanide cations.

log K_{MHL} values are fairly constant along the lanthanide series. The stability trends for Ln^{III} complexes in aqueous solution usually fall within one of the following categories: (i) in the most common case, such as in EDTA complexes, the stability constants increase from La^{III} to Lu^{III};[14] (ii) the stability increases across the series, reaches a plateau, then declines (i.e., DTPA complexes);[15] (iii) with very few ligands, the stability decreases along the lanthanide series.[16] The log K_{ML} values obtained for **L** complexes (Figure 2) indicate that they fall within the second category. As a consequence, the log K_{ML} values obtained for the **L** complexes with the largest Ln^{III} ions investigated (Ln = La,

(12) (a) Lacoste, R. G.; Christoffers, G. V.; Martell, A. E. *J. Am. Chem. Soc.* **1965**, *87*, 2385. (b) Martell, A. E.; Motekaitis, R. J.; Smith, R. M. *NIST Critically Selected Stability Constants of Metal Complexes Database*, version 8.0 for windows; National Institute of Standards and Technology, Standard Reference Data Program: Gaithersburg, MD, 2004.
(13) Costa, J.; Tóth, É.; Helm, L.; Merbach, A. E. *Inorg. Chem.* **2005**, *44*, 4747.
(14) (a) Caravan, P.; Hedlund, T.; Liu, S.; Sjöberg, S.; Orvig, C. *J. Am. Chem. Soc.* **1995**, *117*, 11230. (b) Chapon, D.; Morel, J.-P.; Delangle, P.; Gateau, C.; Pécaut, J. *Dalton Trans* **2003**, 2745.
(15) Sarka, L.; Bányai, I.; Brücher, E.; Király, R.; Platzek, J.; Radüchel, B.; Schmitt-Willich, H. *J. Chem. Soc., Dalton Trans.* **2000**, 3699.
(16) Chang, C. A.; Rowland, M. E. *Inorg. Chem.* **1983**, *22*, 3866.

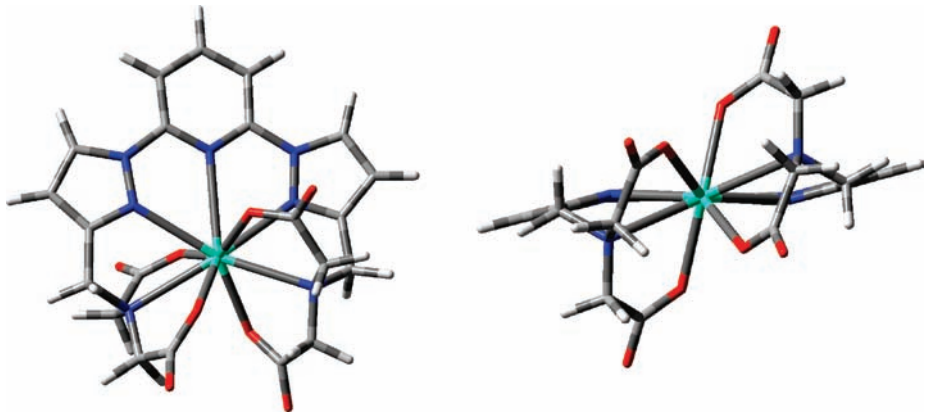

Figure 3. Two views of the minimum energy conformation for the $[Eu\mathbf{L}]^-$ system obtained from B3LYP/6-31G(d) calculations in aqueous solution.

Nd, and Eu) are only slightly lower than those determined for EDTA, while for Lu^{III}, the log K_{ML} value of the EDTA complex is clearly higher than that of the **L** complex. The increased stability of lanthanide complexes often observed across the series is attributed to the increase of charge density of the metal ions. Thus, the stability trend observed for **L** complexes suggests a better match between the binding sites offered by the ligand structure and the binding sites required by large Ln^{III} ions, which results in a drop of the complex stability for the small lanthanides.

The thermodynamic stability constants alone are not sufficient to compare different complex stabilities under physiological conditions. Moreover, the comparison of stability constants of complexes with different stoichiometries is meaningless. The conditional stability constants, or more frequently the pM values, are considered to give a more realistic picture of complex stability. The pM values are usually defined as

$$pM = -\log[M]_{free} \text{ at pH} = 7.4 \text{ for } [M^{III}] = 1\ \mu M,\ [L] = 10\ \mu M$$

The pM values obtained under these conditions for **L** complexes are compared to those of EDTA complexes in Table 1. The data show that the pM values of **L** complexes are only slightly lower than those of EDTA complexes for the largest Ln^{III} ions (La, Nd, and Eu), while for the heaviest Ln^{III} ions, the calculated pM values clearly indicate that the **L** complexes are less stable than the EDTA ones.

Molecular Geometries. Rodríguez-Ubis et al. have used luminescence lifetime measurements to determine the number of inner-sphere water molecules (q) on the Eu^{III} and Tb^{III} complexes of **L**, which provided q values of 0.1−0.2 (Eu) and 0.0−0.1 (Tb),[10b] when taking into account the second sphere interactions according to the treatment of Parker et al.[17] These results indicated that there are no inner-sphere water molecules coordinated to the Ln^{III} ion within experimental error. To gather information on the solution structure of the Ln^{III} complexes of **L**, we have characterized the $[Ln\mathbf{L}]^-$ systems (Ln = La, Nd, Eu, Ho, Yb, or Lu) by means of DFT calculations (B3LYP model) both in vacuo and in aqueous solution. The effective core potential (ECP) of Dolg et al.[18] and the related [5s4p3d]-GTO valence basis set were applied in these calculations. This ECP includes 46 + $4f^n$ electrons in the core, leaving the outermost 11 electrons to be treated explicitly, and it has been demonstrated to provide reliable results for several lanthanide complexes with both macrocyclic[19,20] and acyclic[21] ligands. Compared to all-electron basis sets, ECPs account to some extent for relativistic effects, which are believed to become important for the elements from the fourth row of the periodic table.

Our DFT calculations provide a minimum energy conformation with nearly undistorted C_2 symmetry in which the Ln^{III} is nine-coordinate, being directly bound to the nine available donor atoms of the ligand (Figure 3). The pyrazolyl rings are predicted to be slightly out of coplanarity with respect to the pyridine ring (15.4−16.2° as obtained from the molecular geometries optimized in aqueous solution) in order to decrease the steric demand between protons H2 and H4 (see Scheme 1 for atom numbering). Two of the acetate groups of the ligand are placed clearly above and below the plane of the aromatic tridentate unit of the ligand, while the remaining two acetate pendants are situated only slightly above (or below) that plane. The conformation adopted by the four acetate pendant arms induces chirality in the $[Ln\mathbf{L}]^-$ complexes, so that two enantiomeric forms of the complexes are possible (absolute configuration Δ or Λ).[22]

The calculated bond lengths between the metal ion and the donor atoms of the ligand decrease along the lanthanide series (Table 2), as is usually observed for Ln^{III} complexes as a consequence of the so-called lanthanide contraction.[23] The in vacuo optimized geometries exhibit bond lengths $Ln-N_{PY}$ and $Ln-N_{PYZ}$ (N_{PY} = pyridyl nitrogen atoms, N_{PYZ} = pyrazolyl nitrogen atoms) that are longer than those usually observed for nine-coordinate complexes with tridentate

(17) Beeby, A.; Clarkson, I. M.; Dickins, R. S.; Faulkner, S.; Parker, D.; Royle, L.; de Sousa, A. S.; Wlliams, J. A. G.; Woods, M. *J. Chem. Soc. Perkin Trans. 2* **1999**, 493.

(18) Dolg, M.; Stoll, H.; Savin, A.; Preuss, H. *Theor. Chim. Acta* **1989**, *75*, 173.

(19) Gonzalez-Lorenzo, M.; Platas-Iglesias, C.; Avecilla, F.; Faulkner, S.; Pope, S. J. A.; de Blas, A.; Rodriguez-Blas, T. *Inorg. Chem.* **2005**, *44*, 4254.

(20) Cosentino, U.; Villa, A.; Pitea, D.; Moro, G.; Barone, V.; Maiocchi, A. *J. Am. Chem. Soc.* **2002**, *124*, 4901.

(21) Quali, N.; Bocquet, B.; Rigault, S.; Morgantini, P.-Y.; Weber, J.; Piguet, C. *Inorg. Chem.* **2002**, *41*, 1436.

(22) Jensen, K. A. *Inorg. Chem.* **1970**, *9*, 1.

(23) Seitz, M.; Oliver, A. G.; Raymond, K. N. *J. Am. Chem. Soc.* **2007**, *129*, 11153.

Table 2. Bond Lengths (Å) of the Metal Coordination Environment of Calculated Structures for $[LnL]^-$ Complexes at the B3LYP/6-31G(d) Level[a]

	La		Nd		Eu	
	in vacuo	in solution	in vacuo	in solution	in vacuo	in solution
Ln−N_{PY}	3.093	2.992	3.035	2.937	2.993	2.903
Ln−N_{PYZ}	2.804	2.713	2.742	2.658	2.695	2.622
Ln−N_{AM}	2.856	2.869	2.799	2.814	2.758	2.777
Ln−O_O	2.481	2.498	2.424	2.440	2.376	2.394
Ln−O_I	2.444	2.483	2.392	2.437	2.348	2.392
	Ho		Yb		Lu	
	in vacuo	in solution	in vacuo	in solution	in vacuo	in solution
Ln−N_{PY}	2.953	2.858	2.932	2.838	2.928	2.833
Ln−N_{PYZ}	2.647	2.574	2.618	2.547	2.610	2.542
Ln−N_{AM}	2.718	2.745	2.695	2.725	2.688	2.716
Ln−O_O	2.320	2.338	2.281	2.299	2.269	2.287
Ln−O_I	2.296	2.338	2.261	2.302	2.249	2.292

[a] N_{PY} = pyridyl nitrogen atoms, N_{PYZ} = pyrazolyl nitrogen atoms, N_{AM} = amine nitrogen atoms, O_O = out-of-plane carboxylate oxygen atoms, and O_I = in-plane carboxylate oxygen atoms.

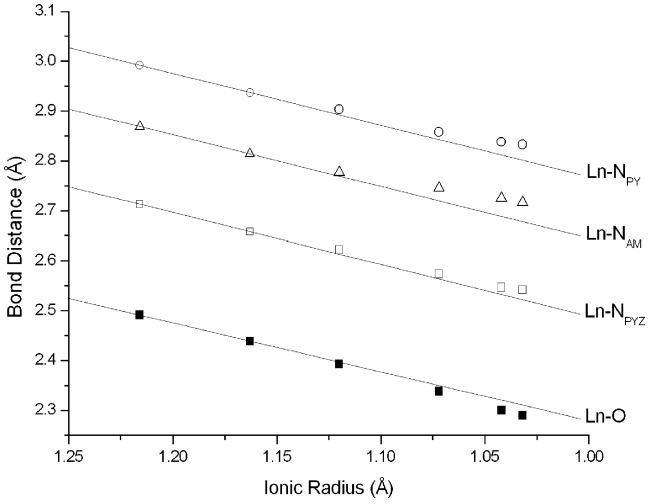

Figure 4. Bond distances of the metal coordination environment obtained in aqueous solution for the $[LnL]^-$ complexes at the B3LYP/6-31G(d) level. The solid lines were calculated by assuming a linear variation with ionic radius of the distances calculated for the La^{III} complex (see text). N_{PY} = pyridyl nitrogen atoms, N_{PYZ} = pyrazolyl nitrogen atoms, N_{AM} = amine nitrogen atoms, O = carboxylate oxygen atoms.

chelating units such as terpy,[24] while the Ln−O bond distances are close to those observed in nine-coordinate Ln^{III} complexes with polyamino carboxylate ligands.[6] In solution, the Ln−N_{PY} and Ln−N_{PYZ} bond distances are shorter than in the gas phase by ca. 0.10 and 0.07 Å, respectively, while the Ln−O bond lengths are slightly increased, providing a better agreement with typical experimental values obtained for Ln^{III} complexes in the solid state.

The variation of the bond distances of the metal coordination environments along the lanthanide series provides some insight into the drop of the metal complex stability for the smallest Ln^{III} ions. Figure 4 shows the bond distances optimized in aqueous solution for the different $[LnL]^-$ complexes together with those estimated by using the ionic radii reported by Shannon for coordination number nine[25] and the bond distances optimized in aqueous solution for the La^{III} complex. For an isostructural series of Ln^{III} complexes with purely electrostatic interactions, one would expect a linear variation of the Ln−donor bond distances with the ionic radius of the Ln^{III} ion. However, the results shown in Figure 4 clearly indicate that the Ln−N bond distances experiment a positive deviation as the ionic radius of the metal ion decreases; that is, these distances are longer than expected taking into account the variation in ionic radius along the series. To compensate for this effect, the Ln−O bond distances experience a negative deviation as the ionic radius of the metal ion decreases. These results suggest that the bis(pyrazolyl)pyridine binding unit provides a good fit with the large Ln^{III} ions, but when the ionic radius decreases, the volume of the complexing cavity becomes too large for the cations, which are displaced toward the stronger coordinating carboxylate entities. The stability trend observed across the lanthanide series from La to Ho for $[LnL]^-$ complexes follows the conventional behavior, with a maximum being observed close to Ho, for which the balance between the fit of the cavity and the steric constraints is optimum. For smaller lanthanide cations, the electrostatic interactions with the carboxylate oxygen atoms appear to be dominant, at the expense of the coordination with the heterocyclic nitrogen atoms, which decreases the stability of the assembly, as pointed out by the potentiometric measurements described above.

^{1}H and ^{13}C NMR Spectra of the Diamagnetic Complexes. The ^{1}H and ^{13}C NMR spectra of the diamagnetic La^{III} and Lu^{III} complexes of **L** were obtained in D_2O solution at pD = 7.5. The ^{1}H spectrum of the La^{III} complex recorded at 300 K shows only seven signals (Figure S2, Supporting Information), which suggests an effective C_{2v} symmetry of the complex in solution. This is confirmed by the ^{13}C spectrum, which consists of nine signals for the 22 carbon nuclei of the ligand backbone (Figure 5). The assignments of the proton signals (Table 3) were based upon heteronuclear multiple-quantum coherence (HMQC) and heteronuclear multiple-bond correlation (HMBC) 2D heteronuclear experiments as well as standard 2D homonuclear correlation spectroscopy (COSY) experiments. The H8 protons (see Scheme 1 for atom numbering) show an AB pattern (^2J = 16.4 Hz) with signals at 3.65 and 3.38 ppm. The specific assignment of these signals to the nuclei in the axial or equatorial position was carried out using the stereochemically dependent proton shift effects, resulting from the polarization of the C−H bonds by the electric field generated by the cation charge. This results in a deshielding of the equatorial protons, which are pointing away from the metal ion.[26]

The proton spectrum of the Lu^{III} complex recorded at 300 K (Figure S3, Supporting Information) consists of 10 signals corresponding to 10 magnetically nonequivalent proton environments in the ligand, which points to an effective C_2

(24) Berthet, J.-C.; Miquel, Y.; Iveson, P. B.; Nierlich, M.; Thuéry, P.; Madic, C.; Ephritikhine, M. *J. Chem. Soc., Dalton Trans.* **2002**, 3265.
(25) Shannon, R. D. *Acta Crystallogr.* **1976**, *A32*, 751.
(26) Gonzalez-Lorenzo, M.; Platas-Iglesias, C.; Avecilla, F.; Geraldes, C. F. G. C.; Imbert, D.; Bünzli, J.-C. G.; de Blas, A.; Rodríguez-Blas, T. *Inorg. Chem.* **2003**, *42*, 6946.

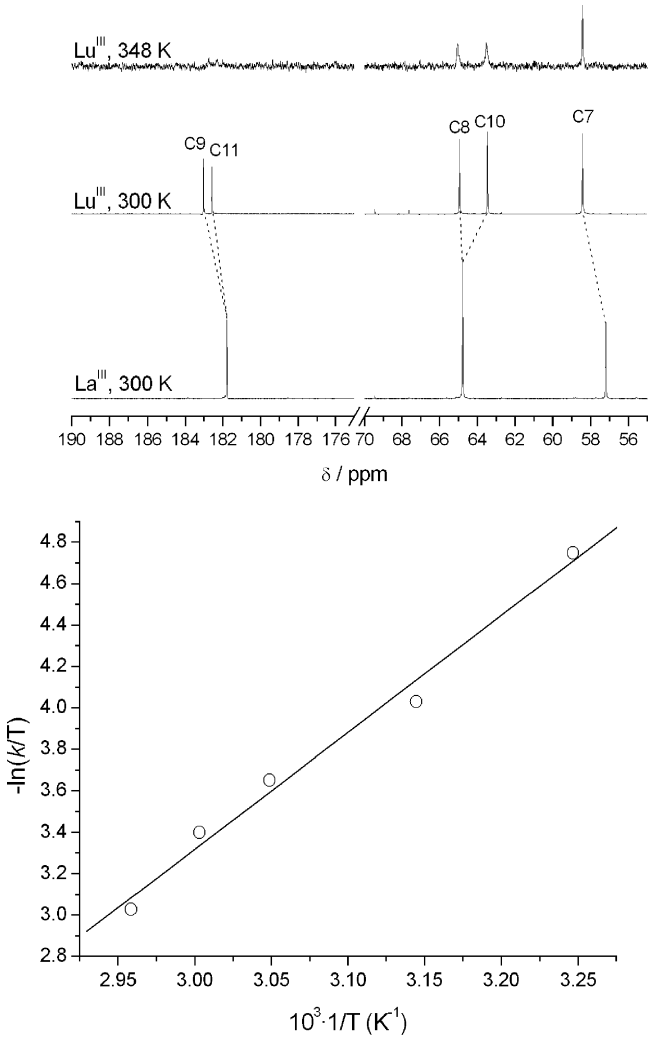

Figure 5. (Top) Partial ^{13}C-{H} NMR spectra of the Lu^{III} and La^{III} complexes of **L** recorded in D_2O solution (pD = 7.5). See Scheme 1 for labeling. (Bottom) Eyring plot for the $\Delta \leftrightarrow \Lambda$ enantiomerization in [Lu**L**]$^-$ based upon line-broadening data for C11.

symmetry of the complex in solution. This is also confirmed by the ^{13}C NMR spectrum, which shows 11 peaks for the 22 carbon nuclei of the ligand backbone (Figure 5). Thus, the ^{1}H and ^{13}C NMR spectra of [Lu**L**]$^-$ show different signals for the in-plane and out-of-plane acetates with respect to the average plane formed by the donor atoms of the bis((pyrazol-1-yl)pyridine unit and the Lu^{III} ion. A specific assignment of the resonances due to in-plane and out-of-plane acetate groups was not possible on the basis of the two-dimensional spectra. To aid the experimental NMR assignments, the ^{13}C NMR shielding constants of [Lu**L**]$^-$ were calculated by using the GIAO method[27] on the DFT calculated structure optimized in aqueous solution (*vide supra* and Experimental Section). It has been reported that calculation of the NMR shielding constants using the 46 + 4f^{14} core electron of Dolg et al.[18] provides inconsistent ^{13}C NMR chemical shifts.[20] Thus, in these calculations, we used the ECP of Stevens et al.,[28,29] which leaves the 4f^{14} electrons in the valence. This

Table 3. ^{1}H and ^{13}C NMR Shifts (ppm with Respect to TMS) for [Ln**L**]$^-$ Complexes (See Scheme 1 for Labeling)[a]

	La^{III}	Lu^{III}		La^{III}	Lu^{III}	
^{1}H	$\delta_{i,exp}$[b]	$\delta_{i,exp}$[c]	^{13}C	$\delta_{i,exp}$[b]	$\delta_{i,exp}$[c]	$\delta_{i,scal}$[d]
H1	8.17	8.16	C1	146.2	146.3	143.2
H2	7.65	7.65	C2	110.4	109.6	106.8
H4	8.39	8.46	C3	150.0	148.5	150.3
H5	6.61	6.65	C4	132.0	133.8	133.5
H7	3.94	3.92	C5	110.5	110.4	107.0
H8ax	3.38	3.65	C6	154.9	156.3	153.8
H8eq	3.65	3.65	C7	57.2	58.4	58.2
H10ax	3.38	3.27	C8	64.8	64.9	67.9
H10eq	3.65	3.80	C9	181.8	183.0	186.8
			C10	64.8	63.5	65.7
			C11	181.8	182.6	184.2

[a] Proton and carbon nuclei of in-plane acetate groups are labeled as H8, C8, and C9, while those corresponding to out-of-plane acetate groups are denoted as H10, C10, and C11. [b] Assignment supported by 2D COSY, NOESY, HMQC, and HMBC experiments at 300 K; $^2J_{8ax,8eq}$ = 16.4 Hz. A single NMR signal is observed for several pairs of nuclei as a consequence of fast $\Delta \leftrightarrow \Lambda$ enantiomerization: H8ax−H10ax, H8eq−H10eq, C8−C10, and C9−C11. [c] Assignment supported by 2D COSY, NOESY, HMQC, and HMBC experiments at 300 K; $^3J_{1,2} = {}^3J_{2,1}$ = 8.1 Hz; $^3J_{4,5} = {}^3J_{5,4}$ = 2.8 Hz; $^2J_{8ax,8eq}$ = 17.5 Hz. [d] Scaled theoretical chemical shift values obtained from GIAO calculations.

method has been shown to provide theoretical ^{13}C NMR shifts in good agreement with the experimental values for different La^{III} and Lu^{III} complexes.[19,20] The main results of these calculations together with the experimental values are given in Table 3. As previously observed for other Ln^{III} complexes,[30] we notice a systematic deviation to lower fields of the calculated values with respect to the experimental ones. Thus, we have plotted the experimental ^{13}C chemical shift values versus the corresponding GIAO calculated ^{13}C chemical shifts, which provides calculated scaled theoretical chemical shift values ($\delta_{i,scal}$) obtained as $\delta_{i,scal} = (\delta_{i,calc} - A)/B$,[31] where $\delta_{i,calc}$ are the GIAO calculated chemical shifts, and A and B are the intercept and slope obtained from the linear correlation plot ($R^2 > 0.998$). The $\delta_{i,scal}$ values are in good agreement with the experimental values, thereby confirming the spectral assignments. These results also indicate that the calculated structure for [Lu**L**]$^-$ provides a good model for the structure of the complex in solution. Once the ^{13}C NMR signals were assigned, a full assignment of the ^{1}H NMR signals was obtained from the cross-peaks observed in the two-dimensional HSQC experiment. Our results indicate that the ^{13}C NMR signals of the in-plane acetate groups (labeled as C8 and C9) are more deshielded than those corresponding to out-of-plane acetate groups (C10 and C11).

For [Lu**L**]$^-$, the ^{13}C NMR signals corresponding to the carbon nuclei C8, C9, C10, and C11 gradually broaden upon increasing the temperature above 300 K, while the remaining carbon signals are not affected. This reflects the presence in solution of a conformational exchange process that can be attributed to a concerted rotation of the glycinate chelate rings during the $\Delta \leftrightarrow \Lambda$ enantiomerization. When the temperature is increased to ca. 348 K, coalescence of the peaks due to

(27) Ditchfield, R. *Mol. Phys.* **1974**, *27*, 789.
(28) Stevens, W. J.; Krauss, M.; Basch, H.; Jaisen, P. G. *Can. J. Chem.* **1992**, *70*, 612.
(29) Cundari, T. R.; Stevens, W. *J. Chem. Phys.* **1993**, *98*, 5555.
(30) Mato-Iglesias, M.; Balogh, E.; Platas-Iglesias, C.; Tóth, É.; de Blas, A.; Rodríguez-Blas, T. *Dalton Trans.* **2006**, 5404.
(31) Barone, G.; Gomez-Paloma, L.; Duca, D.; Silvestre, A.; Riccio, R.; Bifulco, G. *Chem.—Eur. J.* **2002**, *8*, 3233.

C9 and C11 is observed, whereas when the signals due to C8 and C10 are severely broadened, coalescence of these resonances occurs at higher temperatures (Figure 5). These results are consistent with the presence of a single species in solution with C_{2v} symmetry at high temperatures. The rotation of the glycinate chelate rings exchanges protons H8ax−H10ax and H8eq−H10eq, as well as carbons C8−C10 and C9−C11. This process is fast on the NMR time scale at room temperature in the case of the La^{III} complex, which results in an affective C_{2v} symmetry in solution. Thus, there is an increasing rigidity of the complexes in solution on decreasing the ionic radius of the metal ion, as previously observed for other Ln^{III} complexes.[32]

If it is assumed that the exchange process associated with the line broadening (before coalescence) is slow on the NMR time scale, then the exchange rate for this dynamic process (k) can be calculated from $\Delta\nu_{1/2}$, the observed linewidths at half height: $k = \pi(\Delta\nu_{1/2} - \Delta\nu_{1/2}(0))$, where $\Delta\nu_{1/2}(0)$ is the line width in the absence of exchange. A band-shape analysis was carried out on the C11 resonance over the 308−338 K temperature range in order to calculate the activation parameters for the $\Delta \leftrightarrow \Lambda$ interconversion process. An Eyring plot ($R^2 > 0.993$, Figure 5) of $\ln(k/T)$ versus $1/T$ [$k = \chi(k_bT/h)\exp(\Delta S^{\#}/R - \Delta H^{\#}/RT)$, where χ is the transmission coefficient assumed to be 1; k_b is the Boltzmann constant; T is the absolute temperature; k is the rate constant; and $\Delta G^{\#}$, $\Delta H^{\#}$, and $\Delta S^{\#}$ are the activation free energy, enthalpy, and entropy, respectively] yields the following activation parameters: $\Delta G^{\#} = 72.1 \pm 7.9$ kJ mol^{-1}, $\Delta H^{\#} = 46.9 \pm 3.2$ kJ mol^{-1}, and $\Delta S^{\#} = -84.6 \pm 7.3$ J K^{-1} mol^{-1}, $k = 1.47 \pm 0.15$ s^{-1} at 298 K). In principle, no acetate bond breakage is required for $\Delta \leftrightarrow \Lambda$ interconversion, since this process can proceed by an entirely intramolecular twist-type mechanism in which individual chelate rings change chirality via pseudorotational pathways. Detailed studies on EDTA complexes with different 3d metal ions has led to the conclusion that the $\Delta \leftrightarrow \Lambda$ interconversion process occurs via a seven-coordinate intermediate.[33] The negative activation entropy obtained for the $\Delta \leftrightarrow \Lambda$ racemization in [Lu**L**]$^-$ indicates an associatively activated mechanism, which suggests that this process is assisted by the coordination of a water molecule. This hypothesis is also in excellent agreement with the fast $\Delta \leftrightarrow \Lambda$ racemization observed for the La^{III} complex, as the larger ionic radius of La^{III} ion results in a decreased steric compression around the metal ion in the [La**L**]$^-$ complex. As a result, the metal ion is more easily accessed by an incoming water molecule for large Ln^{III} ions.

Yb^{III}-Induced Paramagnetic Shifts. The binding of a ligand to a paramagnetic Ln^{III} ion generally results in large NMR frequency shifts of the ligand nuclei, with magnitudes and signs depending on both the nature of the lanthanide ion and the relative positions of the nuclei to the metal center.[34] Thus, the analysis of the NMR spectra of Ln^{III} paramagnetic complexes can provide useful structural information in solution. The ^{1}H NMR spectrum of the [Yb**L**]$^-$ complex recorded at 300 K (pD = 7.5) shows 10 signals, in agreement with the effective C_2 symmetry in solution observed for the Lu^{III} analogue (Figure 6). The assignments of the proton signals (Table 4) were based on standard 2D homonuclear COSY experiments, which gave strong cross-peaks between the geminal CH_2 protons, between ortho-coupled pyridyl protons (H1−H2), and between the protons of the pyrazolyl unit (H4−H5). The six ^{1}H NMR peaks due to protons H7, H8, and H10 can be grouped into two different

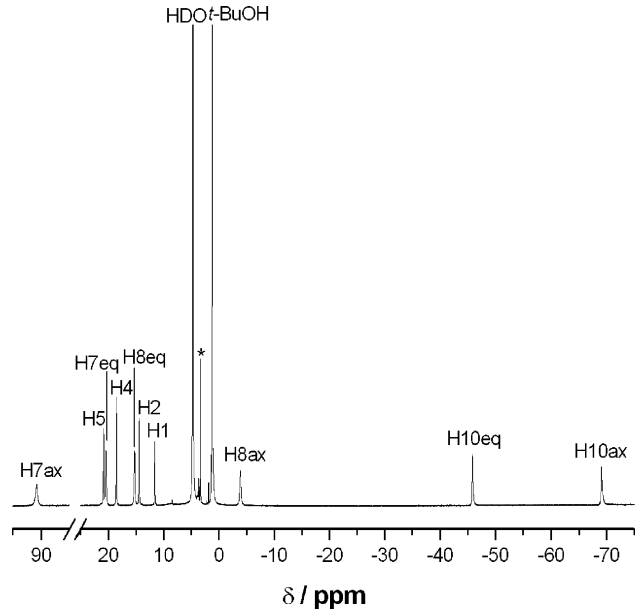

Figure 6. ^{1}H NMR spectrum (300 MHz) of [Yb**L**]$^-$ recorded in D_2O solution at 300 K. The asterisk denotes a diamagnetic impurity.

Table 4. ^{1}H NMR shifts (ppm) for [Yb**L**]$^-$ and experimental and calculated Yb^{III}-induced paramagnetic shifts.[a]

	δ_i^{obs}	δ_i^{para} exptl.[b]	δ_i^{para} calcd.[c]	δ_i^{para} calcd.[d]
H1	11.60	−3.44	−2.47	−3.74
H2	14.44	−6.79	−5.66	−7.68
H4	18.55	−10.09	−8.33	−11.25
H5	20.81	−14.16	−11.14	−13.45
H7ax	90.77	−86.85	−80.08	−84.01
H7eq	20.39	−16.47	−18.14	−16.88
H8ax	−3.89	7.54	10.23	9.66
H8eq	15.23	−11.58	−13.03	−13.76
H10ax	−69.12	72.39	83.65	76.71
H10eq	−45.88	49.68	38.83	46.18
D_1			−385 ± 124	−561 ± 55
D_2			5131 ± 156	5842 ± 70
AF_j			0.1405	0.0564

[a] Assignment supported by 2D COSY experiments at 300 K. Proton nuclei of in-plane acetate groups are labeled as H8, while those corresponding to out-of-plane acetate groups are denoted as H10. [b] The diamagnetic contribution was estimated from the shifts observed for the Lu^{III} analogue. Positive values correspond to shifts to higher fields. [c] Values calculated with the structure of [Yb**L**]$^-$ optimized in vacuo at the B3LYP/6-31G(d) level. [d] Values calculated with the structure of [Yb**L**]$^-$ optimized in aqueous solution at the B3LYP/6-31G(d) level.

(32) (a) Platas-Iglesias, C.; Mato-Iglesias, M.; Djanashvili, K.; Muller, R. N.; Vander Elst, L.; Peters, J. A.; de Blas, A.; Rodríguez-Blas, T. *Chem.—Eur. J.* **2004**, *10*, 3579. (b) Platas, C.; Avecilla, F.; de Blas, A.; Geraldes, C. F. G. C.; Rodríguez-Blas, T.; Adams, H.; Mahía, J. *Inorg. Chem.* **1999**, *38*, 3190. (c) Zucchi, G.; Scopelliti, R.; Pittet, P.-A.; Bünzli, J.-C. G.; Rogers, R. D. *J. Chem. Soc., Dalton Trans.* **1999**, 931.

(33) Maigut, J.; Meier, R.; Zahl, A.; van Eldik, R. *Inorg. Chem.* **2008**, *47*, 5702.

(34) Peters, J. A.; Huskens, J.; Raber, D. J. *Prog. NMR Spectrosc.* **1996**, *28*, 283.

sets according to their relative line broadening: three resonances with linewidths at half height of 46−76 Hz (at 300 MHz and 300 K) and three signals with linewidths in the range 28−35 Hz (Figure 6). These two sets of signals correspond to two sets of Yb^{III}−proton distances, the broader resonances being associated with the protons closer to the metal ion.[35] Thus, the broader resonances were assigned to axial protons, while the second set of signals was assigned to equatorial ones. A full assignment of the ^1H NMR spectrum was achieved with the aid of the Shift Analysis program developed by Forsberg et al.,[36] which includes a function that allows for permutations of the dipolar shifts (see Experimental Section for full details).

For a given nucleus i, the isotropic paramagnetic shift induced by a lanthanide ion j (δ_{ij}^{para}) is a combination of the Fermi contact (δ_{ij}^{con}) and dipolar (δ_{ij}^{dip}) contributions:[34]

$$\delta_{ij}^{para} = \delta_{ij}^{exp} - \delta_i^{dia} = \delta_{ij}^{con} + \delta_{ij}^{dip} \quad (4)$$

where the diamagnetic contribution δ_i^{dia} is obtained by measuring the chemical shifts for analogous diamagnetic complexes (the Lu^{III} complex in the present case). The hyperfine ^1H NMR shifts in Yb^{III} complexes are considered to be largely pseudocontact in origin, and we therefore initiated the analysis of the paramagnetic shifts observed in the ^1H NMR spectrum of the Yb^{III} complex with the assumption that they are dominated by dipolar contributions, as given by the following equation:[34]

$$\delta_{ij}^{dip} = D_1 \frac{3\cos^2\theta - 1}{r^3} + D_2 \frac{\sin^2\theta \cos 2\phi}{r^3} \quad (5)$$

where r, θ, and φ are the spherical coordinates of the observed nucleus with respect to Ln^{III} at the origin and D_1 and D_2 are proportional, respectively, to the axial [$\chi_{zz} - 1/3(\chi_{xx} + \chi_{yy} + \chi_{zz})$] and rhombic ($\chi_{xx} - \chi_{yy}$) anisotropies of the magnetic susceptibility tensor χ. In the special case of axial symmetry, the second term of eq 5 vanishes since $D_2 = 0$.

The analysis of the paramagnetic shifts used to get structural information is generally initiated by assuming a certain structure for the complex in solution, thereby allowing the calculation of the geometric factors. It is frequently assumed that the structure in solution is the same as that determined in the solid state by X-ray crystallography, but an alternative approach is to use molecular[37,38] or quantum mechanical[39] calculations to approximate the structure of a complex. The calculated DFT geometries of $[Yb\mathbf{L}]^-$ optimized both in vacuo and in aqueous solution were used to assess the agreement between the experimental and predicted Yb^{III}-induced paramagnetic shifts with the Shift Analysis program.[36] The Shift Analysis program calculates the dipolar shifts defined by eq 5 in the molecular coordinate system by using a linear least-squares search that minimizes the difference between the experimental and calculated data. The agreement between the experimental and calculated isotropic shifts obtained by using the structure of the complex optimized in vacuo is reasonably good [$AF_j = 0.141$, Table 4]. However, a dramatic improvement of the agreement factor is obtained when the molecular geometry of the complex optimized in aqueous solution is used [$AF_j = 0.056$, Table 4]. Similar agreement factors were previously obtained for axial and nonaxial[40] Yb^{III} complexes according to the dipolar model. These results clearly demonstrate that our DFT calculations provide good models for the structure in solution of the $[Ln\mathbf{L}]^-$ complexes, particularly when solvent effects are taken into account. As expected for a nonaxial system, the D_1 and D_2 values obtained define a very large χ tensor anisotropy, with the z magnetic axis being coincident with the C_2 symmetry axis of the complex.

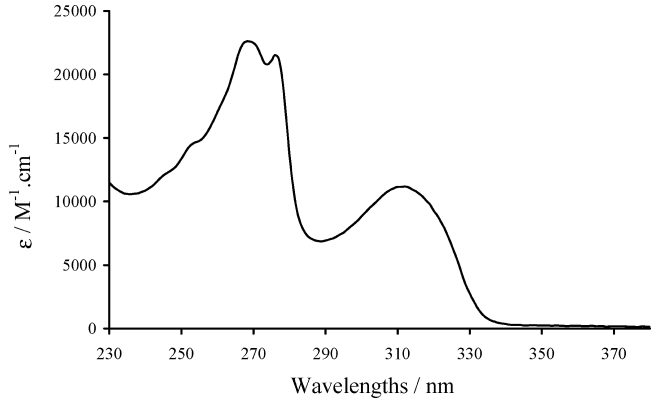

Figure 7. UV−vis absorption spectrum of Na[Er**L**] in TRIS/HCl, 0.01 M, pH = 7.0.

Table 5. Absorpion Properties of the NIR Emitting Complexes in TRIS/HCl, 0.01 M, pH = 7.0

	absorption λ_{max} /nm (ε/M^{-1} cm^{-1})
Nd	311 (13200), 277 (18700), 270 (19300)
Pr	314 (11700), 269 (23100)
Yb	310 (12600), 277 (17500), 269 (17900)
Er	312 (11200), 277 (21300), 269 (22600)

Photophysical Properties. The absorption and emission spectra of several $[Ln\mathbf{L}]^-$ complexes that emit in the visible region (Ln = Sm, Eu, Tb, or Dy) have been reported by Rodríguez-Ubis et al.,[10] who also reported the energy levels of the ligand-centered 0−0 transition for the singlet (33 430 cm^{-1}) and triplet (25 150 cm^{-1}) states in the $[Gd\mathbf{L}]^-$ complex. However, the photophysical properties of $[Ln\mathbf{L}]^-$ complexes that can potentially emit in the near-infrared region remain unexplored. We filled this gap by studying the absorption and emission spectra of the Pr, Nd, Er, and Yb complexes of **L** in aqueous solution. Figure 7 displays the UV−vis spectrum of the Er complex in a buffered water solution (TRIS/HCl, 0.01 M, pH = 7.0), and Table 5 summarizes the absorption properties of the four NIR emitting complexes. All complexes display two strong absorption bands in the UV region at ca. 312 and 270 nm,

(35) Aime, S.; Barbero, L.; Botta, M.; Ermondi, G. *J. Chem. Soc., Dalton Trans.* **1992**, 225.
(36) Forsberg, J. H.; Delaney, R. M.; Zhao, Q.; Harakas, G.; Chandran, R. *Inorg. Chem.* **1995**, *34*, 3705.
(37) Di Bari, L.; Pescitelli, G.; Sherry, A. D.; Woods, M. *Inorg. Chem.* **2005**, *44*, 8391.
(38) Platas-Iglesias, C.; Piguet, C.; Andre, N.; Bünzli, J.-C. G. *J. Chem. Soc., Dalton Trans.* **2001**, 3084.
(39) Fernández-Fernández, M. C.; Bastida, R.; Macías, A.; Pérez-Lourido, P.; Platas-Iglesias, C.; Valencia, L. *Inorg. Chem.* **2006**, *45*, 4484.
(40) Lisowski, J.; Sessler, J. L.; Lynch, V.; Mody, T. D. *J. Am. Chem. Soc.* **1995**, *117*, 2273.

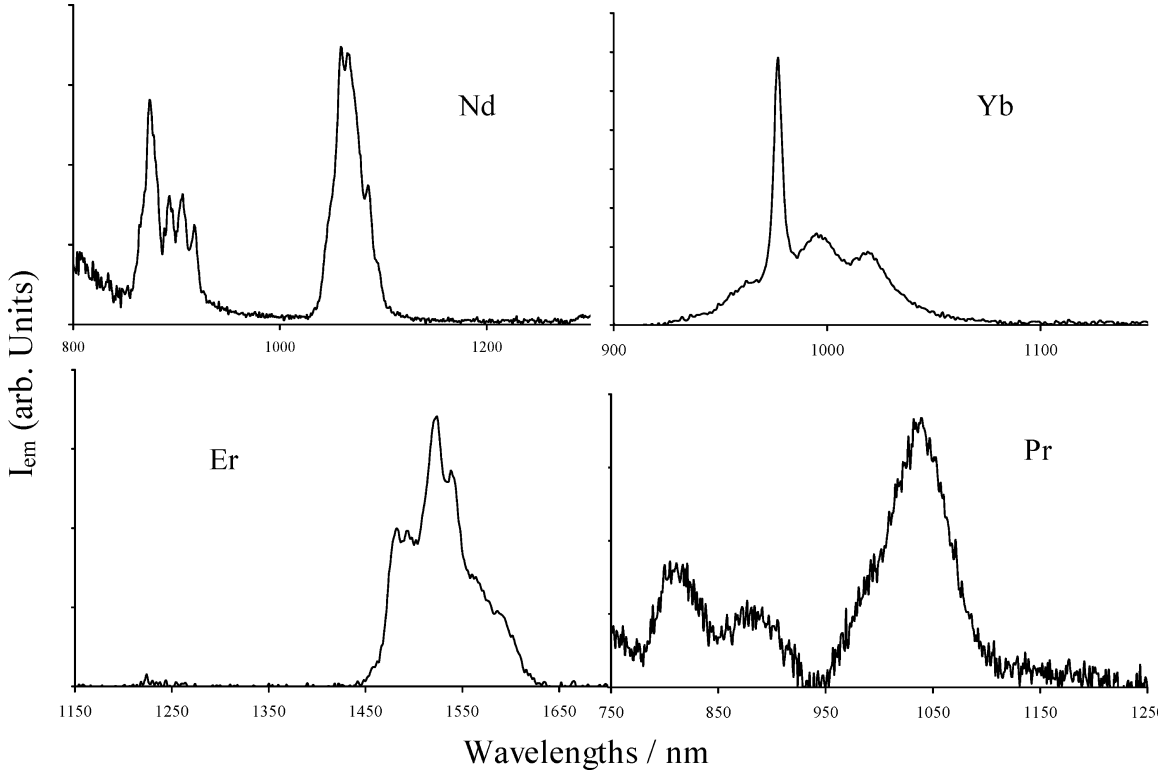

Figure 8. NIR emission spectrum of the Na[Ln**L**] complexes (Ln = Nd, Yb, and Pr in TRIS/HCl 0.01M, pH 7.0) and of Na[ErL] in D_2O.

both being associated with $\pi \rightarrow \pi^*$ transitions on the aromatic moieties.

Upon excitation in the UV region, all of the complexes display emission spectra in the near-infrared region, with emission-line-like spectra characteristic of the used lanthanide. In all cases, the excitation spectra recorded on the f−f transitions matched the absorption spectra, evidencing that the emission arose from energy transfer from the ligand to the metal excited states as a result of the antenna effect.[7,41] Figure 8 displays the NIR emission spectra of the Nd complex from which one can observe the typical transitions from the excited $^4F_{3/2}$ level to the $^4I_{9/2}$ (860 to 930 nm) and $^4I_{11/2}$ (1040 to 1100 nm) levels.[42] The excited-state lifetime was too short to be measured with our instrumental setup. Similarly, excitation of the Yb complex in the UV region leads to the observation of the typical $^2F_{5/2} \rightarrow {}^2F_{7/2}$ emission of Yb,[43] with a maximum at 977 nm (Figure 8). The emission is composed of four transitions arising from the M_J splitting of the fundamental and emitting states due to the ligand field effect,[44] at 9800 (0′−3), 10 050 (0′−2), 10 235 (0′−0), and 10 384 (2′−0) cm^{-1}. The ligand-field splittings amount to 149 cm^{-1} for the $^2F_{5/2}$ level and 245 cm^{-1} for the $^2F_{7/2}$ one. The measured excited-state lifetime of this transition was 3.0 μs in H_2O, a rather significative value compared to other Yb complexes reported in the literature, which generally require the use of D_2O for obtaining submicrosecond lifetimes.[44,45,47] From the metal-centered excited-state lifetime, one can estimate the metal-centered luminescence quantum yield, Φ_{Ln}, using eq 6 and the estimate of the radiative lifetime of Yb, τ_{rad}, determined in organic solvents (2 ms):[46]

$$\Phi_{Ln} = \tau/\tau_{rad} \quad (6)$$

A value of 0.15% was determined, which appeared to be consistent with literature data for Yb complexes in D_2O[44] or in the solid state.[48] Regarding the very large energy gap between the ligand-centered $^3\pi\pi^*$ state (25 150 cm^{-1})[10] and the $^2F_{5/2}$ level of Yb, an efficient sensitization should appear surprising, but it may be explained by the presence of redox processes, as observed in the case of the tryptophan-based sensitization of Yb.[49]

In the case of Er, the emission spectrum was very weak in water and was better evidenced in deuterated water (Figure 8). Upon UV excitation, the emission spectrum of the Er complex showed the typical $^4I_{13/2} \rightarrow {}^4I_{15/2}$ transition of Er,[42]

(41) Alpha, B.; Ballardini, R.; Balzani, V.; Lehn, J.-M.; Perathoner, S.; Sabbatini, N. *Photochem. Photobiol.* **1990**, *52*, 299.
(42) Comby, S.; Bünzli, J.-C. G. *Handbook on the Physics and Chemistry of Rare Earth*; Gschneider, K. A., Jr.; Bünzli, J.-C. G.; Pecharsky, V., Eds.; Elsevier B.V.: Amsterdam, 2007; Vol. *37*, Chapter 235.
(43) Ziessel, R.; Ulrich, G.; Charbonnière, L.; Imbert, D.; Scopelliti, R.; Bünzli, J.-C. G. *Chem.—Eur. J.* **2006**, *12*, 5060.
(44) Goncalves e Silva, F. R.; Malta, O. L.; Reinhard, C.; Güdel, H.-U.; Piguet, C.; Moser, J. E.; Bünzli, J.-C. G. *J. Phys. Chem. A* **2002**, *106*, 1670.
(45) (a) Werts, M. H. V.; Verhoeven, J. W.; Hofstraat, J. W. *J. Chem. Soc., Perkin Trans. 2* **2000**, 1095. (b) Klink, S. I.; Hebbink, G. A.; Grave, L.; Van Veggel, F. C. J. M.; Reinhoudt, D. N.; Sloof, L. H.; Polman, A.; Hofstraat, J. W. *J. Appl. Phys.* **1999**, *86*, 1181.
(46) Hofstraat, J. W.; Oude Wolbers, M. P.; van Veggel, F. C. J. M.; Werts, M. H. V.; Verhoeven, J. W. *J. Fluoresc.* **1998**, *8*, 301.
(47) (a) Quici, S.; Cavazzini, M.; Marzanni, G.; Accorsi, G.; Armaroli, N.; Ventura, B.; Barigeletti, F. *Inorg. Chem.* **2005**, *44*, 529. (b) Comby, S.; Scopelliti, R.; Imbert, D.; Charbonnière, L.; Ziessel, R.; Bünzli, J.-C. G. *Inorg. Chem.* **2006**, *45*, 3158.
(48) Albrecht, M.; Osetska, O.; Klankermayer, J.; Fröhlich, R.; Gumy, F.; Bünzli, J.-C. G. *Chem. Commun.* **2007**, 1834.
(49) Horrocks, W. D., Jr.; Bolender, J. P.; Smith, W. D.; Supkowski, R. M. *J. Am. Chem. Soc.* **1997**, *119*, 5972.

with a maximum at 1524 nm. The luminescence lifetime of this transition was too short to be determined (<1 μs). Finally, the emission spectrum of the Pr complex (Figure 8) displayed weak but measurable emission bands, with a maximum at 1040 cm^{-1} attributed to the $^1D_2 \rightarrow {}^3F_4$ transition.[42]

Conclusion

We have presented a detailed study on the stability, solution structure, and NIR emitting properties of lanthanide complexes with the ligand 2,6-bis{3-[*N*,*N*-bis(carboxymethyl) aminomethyl]pyrazol-1-yl}-pyridine. Potentiometric studies demonstrated that these complexes present stabilities in aqueous solution comparable to those of EDTA for the large Ln^{III} ions, a drop in the stability being observed from Ho to Lu. This stability trend across the lanthanide series has been rationalized by using DFT calculations, which indicate a higher degree of complementarity between the binding sites offered by the ligand structure and the large lanthanides. The conformation that the ligand adopts in the $[Ln\mathbf{L}]^-$ complexes provides chiral Δ or Λ enantiomeric forms. The $\Delta \leftrightarrow \Lambda$ interconversion process is fast on the NMR time-scale for La^{III} but slow at room temperature in the case of the Yb^{III} and Lu^{III} complexes, which clearly indicates an increasing rigidity of the $[Ln\mathbf{L}]^-$ complexes in solution as the ionic radius of the metal ion decreases. The structural models of $[Ln\mathbf{L}]^-$ complexes obtained from DFT calculations performed in aqueous solution are in very good agreement with the experimental solution structure obtained from the analysis of the Yb^{III}-induced paramagnetic shifts. This work demonstrates that theoretical calculations performed at the DFT level in combination with experimental NMR data represent a powerful tool to obtain structural information on lanthanide complexes in solution. Finally, we have also demonstrated that **L** can be used in aqueous solution to sensitize Ln^{III} ions that emit in the NIR spectral region such as Pr^{III}, Nd^{III}, Er^{III}, or Yb^{III}, the latter compound showing a relatively long lifetime in water (3.0 μs).

Experimental Section

Potentiometric Measurements. Ligand protonation constants and stability constants with different Ln^{III} ions (Ln = La, Nd, Eu, Ho, and Lu) were determined by pH-potentiometric titration at 25 °C in 0.1 M KCl. The stock solutions of $LnCl_3$ were prepared from $LnCl_3 \cdot xH_2O$. The samples (8 mL) were stirred while a constant Ar flow was bubbled through the solutions. The titrations were carried out adding a standardized KOH solution with a Metrohm Dosimat 794 automatic burette. A glass electrode filled with 3 M KCl was used to measure pH. The H^+ concentration was obtained from the measured pH values using the correction method proposed by Irving et al.[50] The protonation and stability constants were calculated from parallel titrations with the program PSEQUAD.[51] The errors given correspond to one standard deviation.

NMR Measurements. ^1H and ^{13}C NMR spectra of the diamagnetic La^{III} and Lu^{III} complexes were recorded in D_2O on a Bruker Avance 500 MHz spectrometer. Spectral assignments were based in part on two-dimensional COSY, nuclear Overhauser effect spectrometry (NOESY), HMQC, and HMBC experiments. ^1H NMR spectra of the paramagnetic complexes were recorded on a Bruker Avance 300 spectrometer. All of the NMR spectra recorded in D_2O solution were referenced by using *tert*-butyl alcohol as an internal standard, with the methyl signal calibrated at $\delta = 1.2$ (^1H) and 31.2 ppm (^{13}C). Samples of the complexes for NMR measurements were prepared by dissolving equimolar amounts of the ligand and hydrated $LnCl_3$ in D_2O followed by adjustment of the pD with ND_4OD and DCl (Aldrich) solutions in D_2O.

Lanthanide-induced paramagnetic shifts (LIS) of the $[Yb\mathbf{L}]^-$ complex were calculated using the corresponding Lu^{III} complex as a diamagnetic reference. The LIS values were analyzed with the Shift Analysis program developed by Forsberg et al.,[36] where no assumption is made about the magnetic symmetry of the complex. The in vacuo and in aqueous solution B3LYP-optimized structures of this complex were used as input geometries. The agreement factors between the observed and calculated values were determined according to eq 7:[52]

$$AF_j = \left[\sum_i (\delta_{ij}^{exp} - \delta_{ij}^{cal})^2 / \sum_i (\delta_{ij}^{exp})^2\right]^{1/2} \quad (7)$$

where δ_{ij}^{exp} and δ_{ij}^{cal} represent the experimental and calculated values of a nucleus *i* in a given Ln^{III} complex *j*, respectively.

Computational Methods. All calculations were performed employing hybrid DFT with the B3LYP exchange-correlation functional[53,54] and the Gaussian 03 package (revision C.01).[55] Full geometry optimizations of the $[Ln\mathbf{L}]^-$ systems (Ln = La, Nd, Eu, Ho, Yb, or Lu) were performed in vacuo and in aqueous solution by using the effective core potential of Dolg et al. and the related [5s4p3d]-GTO valence basis set for the lanthanides,[18] and the 6-31G(d) basis set for C, H, N, and O atoms. The stationary points found on the potential energy surfaces as a result of the geometry optimizations performed in vacuo have been tested to represent energy minima rather than saddle points via frequency analysis.

Solvent effects were evaluated by using the polarizable continuum model, in particular employing the integral equation formalism variant.[56] In line with the united atom topological

(50) Irving, H. M.; Miles, M. G.; Pettit, L. *Anal. Chim. Acta* **1967**, *28*, 475.
(51) Zékány L.; Nagypál, I. In *Computation Methods for Determination of Formation Constants*; Leggett, D. J., Ed.; Plenum: New York, 1985; p 291.
(52) Davis, R. E.; Willcott, M. R. *J. Am. Chem. Soc.* **1972**, *94*, 1744.
(53) Becke, A. D. *J. Chem. Phys.* **1993**, *98*, 5648.
(54) Lee, C.; Yang, W.; Parr, R. G. *Phys. Rev. B: Condens. Matter Mater. Phys.* **1988**, *37*, 785.
(55) Frisch, M. J.; Trucks, G. W.; Schlegel, H. B.; Scuseria, G. E.; Robb, M. A.; Cheeseman, J. R.; Montgomery, J. A., Jr.; Vreven, T.; Kudin, K. N.; Burant, J. C.; Millam, J. M.; Iyengar, S. S.; Tomasi, J.; Barone, V.; Mennucci, B.; Cossi, M.; Scalmani, G.; Rega, N.; Petersson, G. A.; Nakatsuji, H.; Hada, M.; Ehara, M.; Toyota, K.; Fukuda, R.; Hasegawa, J.; Ishida, M.; Nakajima, T.; Honda, Y.; Kitao, O.; Nakai, H.; Klene, M.; Li, X.; Knox, J. E.; Hratchian, H. P.; Cross, J. B.; Adamo, C.; Jaramillo, J.; Gomperts, R.; Stratmann, R. E.; Yazyev, O.; Austin, A. J.; Cammi, R.; Pomelli, C.; Ochterski, J. W.; Ayala, P. Y.; Morokuma, K.; Voth, G. A.; Salvador, P.; Dannenberg, J. J.; Zakrzewski, V. G.; Dapprich, S.; Daniels, A. D.; Strain, M. C.; Farkas, O.; Malick, D. K.; Rabuck, A. D.; Raghavachari, K.; Foresman, J. B.; Ortiz, J. V.; Cui, Q.; Baboul, A. G.; Clifford, S.; Cioslowski, J.; Stefanov, B. B.; Liu, G.; Liashenko, A.; Piskorz, P.; Komaromi, I.; Martin, R. L.; Fox, D. J.; Keith, T.; Al-Laham, M. A.; Peng, C. Y.; Nanayakkara, A.; Challacombe, M.; Gill, P. M. W.; Johnson, B.; Chen, W.; Wong, M. W.; Gonzalez, C.; Pople, J. A. *Gaussian 03*, revision C.01; Gaussian, Inc.: Wallingford, CT, 2004.
(56) (a) Cancès, M. T.; Mennucci, B.; Tomasi, J. *J. Chem. Phys.* **1997**, *107*, 3032. (b) Mennucci, B.; Tomasi, J. *J. Chem. Phys.* **1997**, *106*, 5151. (c) Mennucci, B.; Cancès, E.; Tomasi, J. *J. Phys. Chem. B* **1997**, *101*, 10506. (d) Tomasi, J.; Mennucci, B.; Cancès, E. *THEOCHEM* **1999**, *464*, 211.

model,[57] the solute cavity is built as an envelope of spheres centered on atoms or atomic groups with appropriate radii. Calculations were performed using an average area of 0.2 Å^2 for all of the finite elements (tesserae) used to build the solute cavities. For the Ln^{III} ions, the previously parametrized radii were used.[58] Owing to the slow convergence of the geometry optimizations in aqueous solution, some of them (Ln = La, Nd, and Yb) were stopped when the convergence parameters were about twice the default values.[59] For this reason, frequency analysis was not performed to characterize the stationary points; thus, the final geometries obtained for these complexes correspond to stable conformations for the chosen minimization algorithm, rather than true minima. For the remaining $[LnL]^-$ complexes (Ln = Eu, Ho, or Lu), full convergence of the geometry optimizations was achieved. For these complexes, the stationary points found on the potential energy surfaces have been tested to represent energy minima rather than saddle points via frequency analysis. The in vacuo and in aqueous solution optimized Cartesian coordinates of the $[Ln(L)]^-$ systems are given in the Supporting Information.

The NMR shielding tensors (GIAO method)[27] of the $[LuL]^-$ system were calculated in aqueous solution by using the ECP of Stevens et al.[28,29] and the 6-311G(d,p) basis set on ligand atoms. For ^{13}C NMR chemical shift calculation purposes, the NMR shielding tensors of tetramethylsilane (TMS) were calculated at the appropriate level.

Absorption and Emission Spectra. Absorption spectra were recorded in 1 cm^2 quartz suprasil cuvettes on a Shimadzu UV3600 spectrometer. Fluorescence spectra in solutions were measured in 1 cm^2 quartz suprasil cells on a FL 920 Edimburgh instrument equipped with a Hamamatsu R5509-72 photomultiplier for the NIR domain and corrected for the response of the photomultiplier. Steady-state measurements were performed using a continuous 450W Xe arc lamp, while fluorescence lifetimes were determined using a pulsed Xe flashlamp. Decay curves were deconvoluted using the program provided by the supplier, using a solution of silica suspended in water for the measurement of the scattered light.

Synthesis of the Ligand and Complexes. Ligand **L** was obtained by a modification of the reported synthesis,[10] consisting of the alkylation of 2,6-bis-(3-bromomethyl-1-pyrazolyl)pyridine with the ethyl ester of the iminoacetate in place of the *t*-butyl ester.

Synthesis of 2,6-Bis{3-[N,N-bis(ethoxycarbonylmethyl)aminomethyl]pyrazol-1-yl}-pyridine. 2,6-bis-(3-Bromomethyl-1-pyrazolyl)pyridine (764 mg; 1.92 mmol) and diethyl iminodiacetate (0.76 mL; 4.23 mmol) were dissolved in a round-bottom flask containing THF (50 mL) and CH_3CN (100 mL), and K_2CO_3 (1.05 g; 7.68 mmol) was added. The heterogeneous mixture was stirred at 50 °C overnight and filtered hot. The filtrate was concentrated under reduced pressure, and the residual oil was dissolved in DCM (100 mL) and washed with water (3 × 100 mL) and brine (100 mL). The organic phase was dried over Na_2SO_4, filtered, and concentrated to dryness. Flash chromatography over silica gel (CH_2Cl_2/MeOH, 100:00 to 98:2) afforded the pure tetraester (602 mg; 51%) as a white solid. ^1H NMR ($CDCl_3$, 300 MHz): δ 1.22 (t, J = 7.1 Hz, 12H), 3.59 (s, 8H), 4.01 (s, 4H), 4.13 (q, J = 7.1 Hz, 8H), 6.5 (d, J = 2.6 Hz, 2H), 7.75 (s, 1H), 7.78 (m, 2H), 8.45 (d, J = 2.6 Hz, 2H). ^{13}C NMR ($CDCl_3$, 300 MHz): δ 14.2, 51.4, 54.5, 60.5, 108.3, 109.7, 127.8, 141.1, 149.1, 152.9, 171.1. IR (cm^{-1}, ATR): ν 3127 (w), 2982 (w), 2937 (w), 2907 (w), 2874 (w), 1732 (s), 1648 (w), 1606 (m), 1586 (m), 1533 (m), 1470 (s), 1415 (w), 1390 (s), 1283 (m), 1264 (m), 1228 (m), 1186 (s), 1148 (s), 1096 (m), 1072 (w), 1027 (s), 975 (s). Anal. calcd for $C_{29}H_{39}N_7O_8$: C, 56.76; H, 6.41; N, 15.98. Found: C, 56.52; H, 6.21; N, 15.78. FAB$^+$/MS: m/z 614.2 (M + H$^+$, 100%); 526.2 ([M − CH_2COOEt]$^+$, 25%).

Synthesis of L. The tetraethyl ester (602 mg, 0.98 mmol) was dissolved in 30 mL of a MeOH/H_2O (1:1) solution, and NaOH (196 mg, 4.9 mmol) was added. The solution was stirred at 60 °C for 12 h, and the solvents were distilled off. The pale yellow residue was dissolved in 0.5 mL of water and 1 mL of MeOH. Na_4**L** (535 mg, 93%) was precipitated as a white powder with the drop-wised addition of THF. ^1H NMR (D_2O, 300 MHz): δ 3.21 (s, 8H), 3.86 (s, 4H), 6.60 (d, J = 2.3 Hz, 2H), 7.63 (d, J = 8.0 Hz, 2H), 8.04 (t, J = 8.0 Hz, 1H), 8.56 (d, J = 2.3 Hz, 2H).^{13}C NMR (D_2O, 300 MHz): δ 50.3, 57.7, 109.2, 109.9, 129.6, 142.6, 153.0, 153.3, 179.1. IR (cm^{-1}, ATR): ν 3363 (br), 2932 (w), 1575 (s), 1530 (m), 1473 (s), 1401 (s), 1387 (s), 1327 (s) 1286 (m), 1258 (m), 1128 (m), 1049 (m), 982 (m). Anal. calcd for $C_{21}H_{19}N_7O_8Na_4 \cdot 5H_2O$: C, 37.12; H, 4.30; N, 14.43. Found: C, 36.83; H, 4.28; N, 14.28. FAB$^-$/MS: m/z 566.0 ([Na_3**L**]$^-$, 60%), 173.4 ([Na**L**]$^{3-}$, 100%).

Synthesis of the Complexes. Na[NdL]. $Na_4L \cdot 5H_2O$ (20 mg, 29.4 μmol) and $Nd(NO_3)_3 \cdot 6H_2O$ (14.9 mg, 33.9 μmol) were dissolved in water (10 mL). The solution was heated at 60 °C over 4 h. Water was distilled off, and the residue was dissolved in 0.5 mL of water. MeOH, THF, and diethylether were added dropwise, resulting in complex precipitation. Na[Nd**L**] was isolated by centrifugation as a white powder (18.0 mg, 81%). IR (cm^{-1}, ATR): ν 3368 (br), 3147 (w), 3124 (w), 3089 (w), 2929 (w), 2907 (w), 1577 (s), 1534 (m), 1481 (m), 1462 (s), 1390 (s), 1356 (m), 1314 (m), 1258 (m), 1240 (m), 1229 (w), 1175 (w), 1143 (w), 1125 (w), 1100 (w), 1081 (w), 1038 (m), 1003 (m), 996 (m). Anal. calcd for $C_{21}H_{19}NaNdN_7O_8 \cdot 5H_2O$: C, 33.42; H, 3.87; N, 12.99. Found: C, 33.70; H, 3.53; N, 12.86. ESI$^-$/MS: m/z 641.0 ([Nd**L**]$^-$, 100%), 583.2 ([Nd**L**]$^-$ − CH_2CO_2, 25%).

Na[ErL]. In a 25 mL flask containing $Na_4L \cdot 5H_2O$ (20.0 mg, 29.4 μmol) in H_2O (15 mL) was added $Er(NO_3)_3 \cdot 5H_2O$ (15.0 mg, 0.03 mmol) in H_2O (5 mL). The mixture was stirred for 3 h at 60 °C and filtered. The filtrate was concentrated to 1 mL. Successive addition of MeOH, THF, and Et_2O resulted in the formation of a white precipitate, which was isolated by centrifugation to yield Na[Er**L**] (14.4 mg, 66%). IR (cm^{-1}, ATR): ν 1642 (m), 1586 (s), 1539 (m), 1482 (m), 1469 (m), 1447 (w), 1389 (s). Anal. calcd for $C_{21}ErH_{19}NaN_7O_8 \cdot 3H_2O$: C, 34.01; H, 3.40; N, 13.22. Found: C, 33.97; H, 3.44; N, 13.08. ESI$^-$/MS: m/z 663 ([Er**L**]$^-$, 100%), 605.2 ([Er**L**]$^-$ − CH_2CO_2, 25%).

Na[PrL]. $Na_4L \cdot 5H_2O$ (20 mg, 29.4 μmol) and $Pr(OTf)_3$ (19.9 mg, 34 μmol) were dissolved in water (10 mL). The solution was heated at 60 °C over 4 h. Water was distilled off, and the residue was dissolved in 0.5 mL of water. MeOH, THF, and diethylether were added dropwise, resulting in complex precipitation. Na[Pr**L**] was isolated by centrifugation as a white powder (19.3 mg, 89%). IR (cm^{-1}, ATR): ν 3395 (br), 3107 (w), 1586 (s), 1532 (m), 1480 (m), 1460 (s), 1395 (s), 1359 (m), 1336 (m), 1316 (m), 1257 (w), 1235 (w), 1190 (w), 1174 (w), 1144 (w), 1127 (w), 1104 (w), 1080 (m), 1038 (m), 1005 (m). Anal. calcd for $C_{21}H_{19}NaN_7O_8Pr \cdot 4H_2O$: C, 34.39; H, 3.71; N, 13.37. Found: C, 34.22; H, 3.48; N, 13.07.

Na[YbL]. In a 25 mL flask, $Na_4L \cdot 5H_2O$ (20.0 mg, 29.4 μmmol) was dissolved in H_2O (12 mL), and $Yb(NO_3)_3 \cdot 5H_2O$ (15.2 mg, 0.03 mmol) dissolved in H_2O (3 mL) was added. The mixture was stirred for 3 h at 60 °C and filtered. The filtrate was concentrated to 1 mL. Successive addition of MeOH, THF, and Et_2O resulted in the formation of a white precipitate, which was isolated by centrifugation to yield Na[Yb**L**] (11.4 mg, 52%). IR (cm^{-1}, ATR):

(57) Barone, V.; Cossi, M.; Tomasi, J. *J. Chem. Phys.* **1997**, *107*, 3210.
(58) Cosentino, U.; Villa, A.; Pitea, D.; Moro, G.; Barone, V. *J. Phys. Chem. B* **2000**, *104*, 8001.
(59) (a) Cosentino, U.; Moro, G.; Pitea, D.; Barone, V.; Villa, A.; Muller, R. N.; Botteman, F. *Theor. Chem. Acc.* **2004**, *111*, 204. (b) Li, H.; Jensen, J. H. *J. Comput. Chem.* **2004**, *25*, 1449.

ν 1655 (m), 1618 (m), 1586 (s), 1539 (m), 1485 (m), 1470 (m), 1447 (w). Anal. calcd for $C_{21}H_{19}NaN_7O_8Yb \cdot 3H_2O$: C, 33.74; H, 3.37; N, 13.12. Found: C, 33.60; H, 3.15; N, 12.89. ESI^-/MS: *m*/*z* 669.1 ([Yb**L**]$^-$, 100%), 611.0 ([Yb**L**]$^-$ − CH_2CO_2, 15%).

Acknowledgment. The authors are indebted to Centro de Supercomputación de Galicia for providing the computer facilities and to the French Centre National de la Recherche Scientifique for financial support. The support and sponsorship arranged by the EU COST Action D38 "Metal-Based Systems for Molecular Imaging Applications" is also kindly acknowledged. The European Commission is gratefully acknowledged for financial support to M.S. (STREP project POC4Life n°037933).

Supporting Information Available: Potentiometric titration curves of **L** with and without selected Ln^{III} ions, ^1H NMR spectra of Na[Lu**L**] and Na[La**L**] in D_2O, and optimized Cartesian coordinates of the [Ln**L**]$^-$ complexes (Ln = La, Nd, Eu, Ho, Yb or Lu) in vacuo and in water. This material is available free of charge via the Internet at http://pubs.acs.org.

IC801816P